Polymorphism, Structural Frustration, and Electrical Properties of the Mixed Conductor $Ag_{10}Te_4Br_3$

Stefan Lange,[†] Melanie Bawohl,[†] Dirk Wilmer,[‡] Hinrich-Wilhelm Meyer,[‡] Hans-Dieter Wiemhöfer,[†] and T. Nilges*,[†]

Institut für Anorganische und Analytische Chemie and Institut für Physikalische Chemie, Universität Münster, Corrensstrasse 30, D-48149 Münster, Germany

Received November 16, 2006. Revised Manuscript Received December 29, 2006

$Ag_{10}Te_4Br_3$ is polymorphic with four polymorphs in the temperature range from 3 to 450 K. It represents the first member of a formerly unseen class of materials featuring covalently and ionically bonded tellurium substructures. Thermal analyses (DSC and C_p) prove the reversibility of the $\alpha-\beta$, $\beta-\gamma$, and $\gamma-\delta$ phase transitions at 355, 317, and 290 K, respectively. The existence of the low-temperature δ-phase is substantiated by C_p measurements down to 3 K. Temperature-dependent single-crystal structure analysis and nonharmonic refinements of the silver distribution for all polymorphs reveal a high silver mobility over the whole temperature range. A significant change in the dimensionality of the silver distribution, from an exclusively 2D (δ, γ) to a 3D (β, α) arrangement, can be observed for $Ag_{10}Te_4Br_3$ with the increase in temperature. The enhanced silver mobility causes a structural frustration and disorder phenomena of the predominantly covalently bonded tellurium substructure for the high-temperature α- and β-polymorphs. The increase in disorder comes along with the occurrence of diffuse scattering in form of Kagomé nets, indicating a structural frustration in a rod packing arrangement. An ionic conductivity, approaching the values of most of the known silver super ion conductors and only 1 order of magnitude lower than that in $RbAg_4I_5$, are a remarkable feature of air-, photo-, and moisture-stable $Ag_{10}Te_4Br_3$.

1. Introduction

In the past, silver ion conductors have been used for electrochemical gas sensors,[1−2] ion-selective electrodes,[3] microbatteries and coulometric devices,[4] and thermoelectric or magnetic materials; more recently, silver ion conductors were proposed for applications in nanostructured memories. The memory devices are based on the electrochemical control of nanoscale quantities of metal in thin film electrolytes. The development of nonvolatile memory devices is one key step in the exploration of new data storage devices. Silver ion conductor containing compounds play a major role in this development process because of their favorable properties, such as high ion mobility, good cycleability, or low voltage and current characteristics.[5−7]

Focusing on three important classes of crystalline ion conducting silver materials, the binary and ternary silver chalcogenides, silver polychalcogenides, and silver chalcogenidehalides, only a handful of examples can be found for each class. A brief summary with ternary phase diagrams covering those materials is given elsewhere.[8] Silver halides and silver chalcogenides stand at the beginning of solid-state ionics, where they serve to model and test many of the physical effects and applications connected with ion transport and thermodynamics of solid electrolytes and mixed conducting solids. Very early in that development, ternary silver chalcogenidehalides were recognized as key compounds that guarantee the low interface resistance of contacts between mixed conducting silver chalcogenides and silver halides, in particular AgI.[9−11]

Recently, γ-$Ag_{10}Te_4Br_3$, the first and only existing silver polychalcogenidehalide, was discovered by Nilges et al.[8] Some properties were reported in a previous contribution and a more complete characterization is now presented in this paper. A high ion dynamic and a pronounced silver mobility could be observed within the tellurium substructure with significantly enhanced mobility around covalently bonded $[Te_2]^{2-}$ units of the polychalcogenide substructure. Polymorphism is a common phenomenon in fast ion conductors, for instance, $RbAg_4I_5$,[12] and can be also expected from the structural and physical properties of the room-temperature

* Corresponding author. Phone: 49-251-83-36645. Fax: 49-251-83-36002. E-mail: nilges@uni-muenster.de.
[†] Institut für Anorganishe und Analytische Chemie, Universität Münster.
[‡] Institut für Physikalische Chemie, Universität Münster.

(1) Nagashima, K.; Nakano, N. *Zairyo Gijutsu* **1997**, *15*, 146.
(2) Sunu, S. S.; Jayaraman, V.; Prabhu, E.; Gnanasekar, K. I.; Gnanasekaran, T. *Ionics* **2004**, *10*, 244.
(3) Cammann, K.; Galster, H. In *Das Arbeiten mit ionensensitiven Elektroden*, 3rd ed.; Springer: Berlin, 1996.
(4) Takahashi T. In *Handbook of Solid State Batteries & Capacitors*; Prasad, P. S. S., Munshi, M. Z. A., Eds.; World Scientific: Hackensack, NJ, 1995; pp 79−109.
(5) Kozicki, M. N.; Mitkova, M.; Park, M.; Balakrishnan, M.; Gopalan, C. *Superlattices Microstruct.* **2003**, *34*, 459.
(6) Pinnow, C.-U.; Happ T. Patent DE 102004014965.
(7) Pinnow, C.-U.; Mikolajick, T.; Happ, T.; Symanczyk, R. Patent DE 10323414.
(8) Lange, S.; Nilges, T. *Chem. Mater.* **2006**, *18*, 2538.
(9) Owens, B.; Argue, G. R.; Groce, I. J.; Hermo, L. D. *J. Electrochem. Soc.* **1969**, *116*, 312.
(10) Valverde, N. *Z. Phys. Chem. NF* **1971**, *75*, 1.
(11) Rickert, H. In *Electrochemistry of Solids*; Springer: Berlin, 1982.
(12) Funke, K.; Banhatti, R. D.; Wilmer, D.; Dinnebier, R.; Fitch, A.; Jansen, M. *J. Phys. Chem. A* **2006**, *110*, 3010.

10.1021/cm062731p CCC: $37.00
Published on Web 02/17/2007

polymorph. Temperature-dependent structure determinations, impedance spectroscopy, and thermal analyses were performed to verify this assumption.

2. Experimental Section

2.1. Synthesis. Phase-pure bulk material of $Ag_{10}Te_4Br_3$ was prepared from a 7:3:4 mixture (molar ratio) of silver (Chempur, 99.9%), silver(I) bromide (Chempur, 99.9%), and tellurium (Alfa Aesar, 99.9999%). The starting materials were sealed into evacuated silica ampoules, heated to 1270 K, held at this temperature for 1 day, and quenched in an ice bath. The crude product was finely ground and annealed at 620 K for 3 weeks, followed by a slow cooling to room temperature. Further preparation details concerning the single-crystal growth can be found elsewhere.[8] The composition of the single crystals was checked by EDX and the purity of the bulk material by X-ray phase analysis.

2.2. Electron Microprobe Analyses. Semiquantitative analysis was performed with a Leica 420i scanning electron microscope (Zeiss) fitted with an energy dispersive detector unit (EDX, Oxford). Silver, HgTe (Te), and KBr (Br) were used as standards for calibration. A voltage of 20 kV was applied to the samples.

The ideal composition of $Ag_{10}Te_4Br_3$ was substantiated within the accuracy of the applied method. Values in atomic percent Ag 56(2), Te 24(2), and Br 20(2) were averaged from the single crystals in good agreement with the theoretical values of Ag 58.9, Te 23.5, and Br 17.6. Estimated standard deviations are given in parentheses. Small discrepancies in the EDX data are due to the irregularly shaped surface of the single crystals.

2.3. XRD Experiments. X-ray powder diffraction phase analysis was performed to verify the phase purity of $Ag_{10}Te_4Br_3$. Finely ground samples were examined using a Stoe StadiP X-ray powder diffractometer operated with Cu Kα_1 radiation (λ = 1.54051 Å) and equipped with a linear 5° position-sensitive detector (PSD, Braun). Silicon was used as an external standard. A comparison of the measured with calculated powder diffractograms (data from ref 8) substantiated the purity of the samples used for thermal and structural analysis.

Intensity data of two different crystals (crystal 1 used for the 340 and 410 K and crystal 2 for the room temperature and 223 K measurements) were collected on a Stoe-IPDS II imaging plate diffractometer fitted with Mo Kα radiation (λ = 0.71073 Å). Temperature-dependent measurements were done using a Cryostream plus system (Oxford). The temperature was calibrated by measuring the two reversible phase transitions of Ag_5Te_2Cl at 244 and 334 K.[13] A temperature deviation of less than ±0.1 K from the ideal value was achieved during the measurements.

The datasets were corrected for Lorentz and polarization effects. A numerical absorption correction based on optimized crystal shapes, derived from symmetry equivalent reflections, was applied to each data set prior to the structure refinements.[14] The structures were solved by direct methods, implemented in the ShelxS program suite.[15] All space groups were derived from a careful analysis of the extinction rules. Structure refinements were performed using the Jana 2000 program.[16] Precession plots were calculated from the intensity data for each dataset using the Stoe X-area program package.[17]

2.4. Thermal Analyses. A finely ground sample of phase pure $Ag_{10}Te_4Br_3$ (30.74 mg) was transferred to an aluminum crucible and was measured with a rate of 10 K/min using a Netzsch DSC 204 t equipment. Hg, In, Sn, Bi, Zn, and CsCl were used as standards for temperature and enthalpy calibration. All measurements were performed under a N_2 atmosphere. An accuracy of ±0.5 K could be estimated from the calibration measurements. The thermal effects were derived as onset temperatures.

Finely ground $Ag_{10}Te_4Br_3$ was pressed to a pellet and glued to the platform of a precalibrated heat capacity puck of a Quantum design physical property measurement system (PPMS) using Apiezon N grease. C_p measurements have been performed using the C_p option of the PPMS in the temperature range from 150 to 3 K. We could not detect any thermal effect in the applied temperature range, leading to the conclusion that δ-$Ag_{10}Te_4Br_3$, stable at temperatures below 290 K (verified by X-ray structure analyses at 223 and 100 K), is the only existing polymorph down to 3 K.

2.5. Conductivity Measurements. Total conductivities of $Ag_{10}Te_4Br_3$ were measured with a Novocontrol standard sample cell BDS 1200 using a Novocontrol alpha-S impedance analyzer. A frequency range of 3 MHz to 10 mHz was applied in a temperature range of 153−293 K. Ion blocking gold electrodes were sputtered to cold pressed pellets and impedance spectra were recorded under an oxygen and moisture-free nitrogen atmosphere. An equilibration time of 1−5 min was used between each measurement in order to achieve temperature constancy.

A symmetric cell with two electron-blocking but silver-ion-conducting electrodes was used to measure the partial conductivity of silver ions in $Ag_{10}Te_4Br_3$ according to the well-known electrochemical concepts introduced by C. Wagner[18] and applied by many authors since then.[19−24] Electron-blocking electrodes were prepared by cold pressing 6 mm pellets of a mixture of $RbAg_4I_5$, $RbAg_4I_5$/Ag (1:1), and Ag powder in a 6:1:1 volume ratio at 15 kN. $RbAg_4I_5$ was prepared by mixing AgI (powder, Sigma Aldrich, 99%) and RbI (powder, Alfa, 99.8%) in a 4:1 ratio in evacuated quartz ampoules, subsequently heating to 973 K for 1 day and quenching in an ice bath. The phase purity was checked by X-ray powder diffraction. $RbAg_4I_5$ was stored at 323 K prior to use and each electrode was prepared directly before the measurements. The silver-ion-conducting electrodes were contacted on both sides of a cold-pressed $Ag_{10}Te_4Br_3$ pellet achieving the phase sequence $Ag|RbAg_4I_5|Ag_{10}Te_4Br_3|RbAg_4I_5|Ag$. This setup was mounted between Pt electrodes and connected to a Solartron 1287 potentiostat, which was controlled by a Solartron 1260 frequency response analyzer. All measurements were performed under a N_2 atmosphere. Impedance spectra were recorded within a frequency range of 1 MHz to 0.1 Hz applying a temperature range of 300−423 K. One hour of equilibration time was supplied prior to each impedance measurement after reaching a new temperature. The typical impedance spectrum was characterized by the expected frequency dependence of the finite Warburg impedance.[25−27] The

(13) Nilges, T.; Nilges, S.; Pfitzner, A.; Doert, T.; Böttcher, P. *Chem. Mater.* **2004**, *16*, 806.
(14) (a) *X-RED 32*, version 1.10; Stoe & Cie GmbH: Darmstadt, Germany, 2004. (b) *X-SHAPE*, version 2.05; Stoe & Cie GmbH: Darmstadt, Germany, 2004.
(15) Sheldrick, G. M. *SHELXS97*; University of Göttingen: Göttingen, Germany, 1997.
(16) Petricek, V.; Dusek, M.; Palatinus, L. *JANA2000, The Crystallographic Computing System*; Institute of Physics: Praha, Czech Republic, 2000.
(17) *X-area* program package, version 1.25; Stoe & Cie GmbH: Darmstadt, Germany, 2004.
(18) Wagner, C. *J. Chem. Phys.* **1953**, *21*, 1819.
(19) Yokota, I. *J. Phys. Soc. Jpn.* **1961**, *16*, 2213.
(20) Rickert, H.; Wagner, C. *Ber. Bunsenges. Phys. Chem.* **1963**, *67*, 621.
(21) Valverde, N. *Z. Phys. Chem. NF* **1970**, *70*, 128−138.
(22) Bonnecaze, G.; Lichanot, A.; Liotard, D.; Adell, A.; Gromb, S. *J. Phys. Chem. Solids* **1983**, *44*, 95.
(23) Grientschnig, D.; Sitte, W. *Z. Phys. Chem. NF* **1990**, *168*, 143.
(24) Janek, J.; Korte, C. *Solid State Ionics* **1996**, *92*, 193.
(25) Ho, C.; Raistrick, I. D.; Huggins, R. A. *J. Electrochem. Soc.* **1980**, *127*, 343.
(26) Boukamp, B. A.; Wiegers, G. A. *Solid State Ionics* **1983**, *9−10*, 1193.
(27) Rickert, H.; Stroetmann, B.; Wiemhöfer, H.-D. In *6th Riso International Symposium on Metallurgy and Materials Science*; Poulsen, F. W., Ed.; National Laboratory: Roskilde, Denmark, 1985; pp 413.

Table 1. Crystallographic Data for Polymorphic $Ag_{10}Te_4Br_3$

empirical formula	$Ag_{10}Te_4Br_3$				
fw	1828.8				
polymorph	α	*β*	*γ*	*γ*	*δ*
crystal shape and color	isomorphic, dark gray				
cryst size (mm^3)	0.04 × 0.03 × 0.02	0.04 × 0.03 × 0.02	0.07 × 0.06 × 0.06	0.04 × 0.03 × 0.03	0.04 × 0.03 × 0.03
cryst syst	hexagonal	hexagonal	orthorhombic	orthorhombic	orthorhombic
space group (No.)	*P*6/*mmm* (191)	$P6_3/mmc$ (194)	*Cmcm* (63)[8]	*Cmcm* (63)	$Cmc2_1$ (36)
Z	1	6	8	8	8
a (Å)	7.984(2)	13.748(2)	15.374(1)[b]	15.374(1)[b]	15.400(1)
b (Å)			15.772(1)	15.772(1)	15.654(1)
c (Å)	7.688(2)	15.383(2)	13.715(1)	13.715(1)	13.699(1)
V ($Å^3$)	424.4(2)	2518.0(6)	3325.6(4)	3325.6(4)	3302.4(4)
T (K)	410	340	293	293	223
F(000)	784	4701	6264	6264	6264
ρ_{calcd} (g cm^{-3})	7.153	7.239	7.303	7.303	7.354
no. of reflns	3670	13799	27330	10311	14023
no. of independent reflns	250	1180		2115	4080
twin matrices (by rows)			$T_{1/2}$ (1 0 0 0 1/2 3/4 0 −1 1/2); $T_{1/3}$ (1 0 0 0 1/2−3/4 0 1 1/2)	no twinning	inversion twin
refinement method	full matrix least -squares on $F^{2\ 16}$	full matrix least -squares on $F^{2\ 16}$	full matrix least -squares twin (hklf 5) refinement[a] on $F^{2\ 16}$	full matrix least -squares on $F^{2\ 16}$	full matrix least -squares on $F^{2\ 16}$
$R_{\sigma I}$	0.0503	0.1011	0.1096	0.0667	0.0341
no. of params	46	159	159	124	218
final *R* values [$I > 3_{\sigma I}$] *R*1	0.0313	0.0369	0.0605	0.0580	0.0346
*wR*2	0.0644	0.0536	0.0792	0.0629	0.0524
final *R* values [all] *R*1	0.0711	0.1531	0.2211	0.1374	0.0532
*wR*2	0.0713	0.0696	0.0936	0.0688	0.0541
BASF					0.50(3)
largest difference peak and hole (e $Å^{-3}$)	0.94/−0.87	1.48/−2.37	2.41/−1.80	2.31/−1.79	1.65/−1.62

[a] CSD-416031 contains the supplementary crystallographic data for a twin refinement.[8] [b] Lattice parameters are derived from X-ray powder diffraction.

high-frequency limit of the real part of the impedance was determined by the total conductivity of electrons and silver ions. The extrapolated low-frequency value of the impedance (real part), which was higher, as expected, corresponds to the silver ion transport only. After each impedance measurement, a dc measurement was carried out by applying a dc potential difference in the cell and taking the steady-state ionic current after 400 s. The resulting dc resistance was again used to calculate the ionic conductivity. Conductivity values as evaluated from the low-frequency part of the impedance spectra and from the steady-state dc currents agreed well within the experimental errors.

3. Results and Discussion

The following section deals with the structural characterization and the determination of the electrical properties of the first silver(I) polychalcogenidehalide. Temperature-dependent single-crystal structure determinations at various temperatures are reported in order to get a detailed insight in the structural properties of this new material. The complex structural features of the anion and cation substructures are discussed separately, followed by a brief discussion of some disorder phenomena caused by a structural frustration of parts of the anion substructure. Thermal analysis and impedance spectroscopy outline the stability and the electrochemical performance of $Ag_{10}Te_4Br_3$ at various temperatures.

3.1. Structure Refinements. Temperature-dependent structure determinations have been performed within the temperature range of 100−410 K. A total number of five measurements have been done at 100, 223, 293, 340, and 410 K in order to analyze the structural changes undergoing the observed phase transitions. The stability ranges of all polymorphs are reported in the thermal and electrical property section. Four different structures could be identified starting with *δ*-$Ag_{10}Te_4Br_3$ at 223 K to α-$Ag_{10}Te_4Br_3$ at 410 K. A brief summary of all crystallographic details is given in Table 1. The structure determination at 100 K substantiated the occurrence of the *δ*-phase down to this temperature.

Because of the high silver mobility, the silver distribution of all polymorphs was described using a nonharmonic approach. The procedure of nonharmonic refinement[28−31] is well-suited for all ion conducting materials, as it has been shown for many other materials in this field.[32−35] The significance of the third-order terms was checked by an analysis of the joint probability density functions (jpdf) showing negative regions of not more than 5% of the positive pdf values. The maxima of the probability density, the so-called mode positions (suffix m), were determined from the probability density function (pdf) of each nonharmonically refined position. All distance and angle discussions are related to those positions. A brief summary of the refinement strategies and crystallographic aspects is given in the Supporting Information because the possibility of twinning and the occurrence of incommensurate structures had to be verified. We have very carefully checked the existence of satellite or supercell reflections in the datasets because those features have been observed in many other polytelluride

(28) Kuhs, W. F. *Acta Crystallogr., Sect. A* **1992**, *48*, 80.
(29) Willis, B. M. T. *Acta Crystallogr., Sect. A* **1969**, *25*, 277.
(30) Bachmann, R.; Schulz, H. *Acta Crystallogr., Sect. A* **1984**, *40*, 668.
(31) Zucker, U. H.; Schulz, H. *Acta Crystallogr. Sect. A* **1982**, *38*, 563.
(32) Zucker, U. H.; Schulz, H. *Acta Crystallogr., Sect. A* **1982**, *38*, 568.
(33) Nilges, T.; Dreher, C.; Hezinger, A. *Solid State Sci.* **2005**, *7*, 79.
(34) Nilges, T.; Lange, S. *Z. Anorg. Allg. Chem.* **2004**, *630*, 1749.
(35) Nilges, T.; Lange, S. *Z. Anorg. Allg. Chem.* **2005**, *631*, 3002.

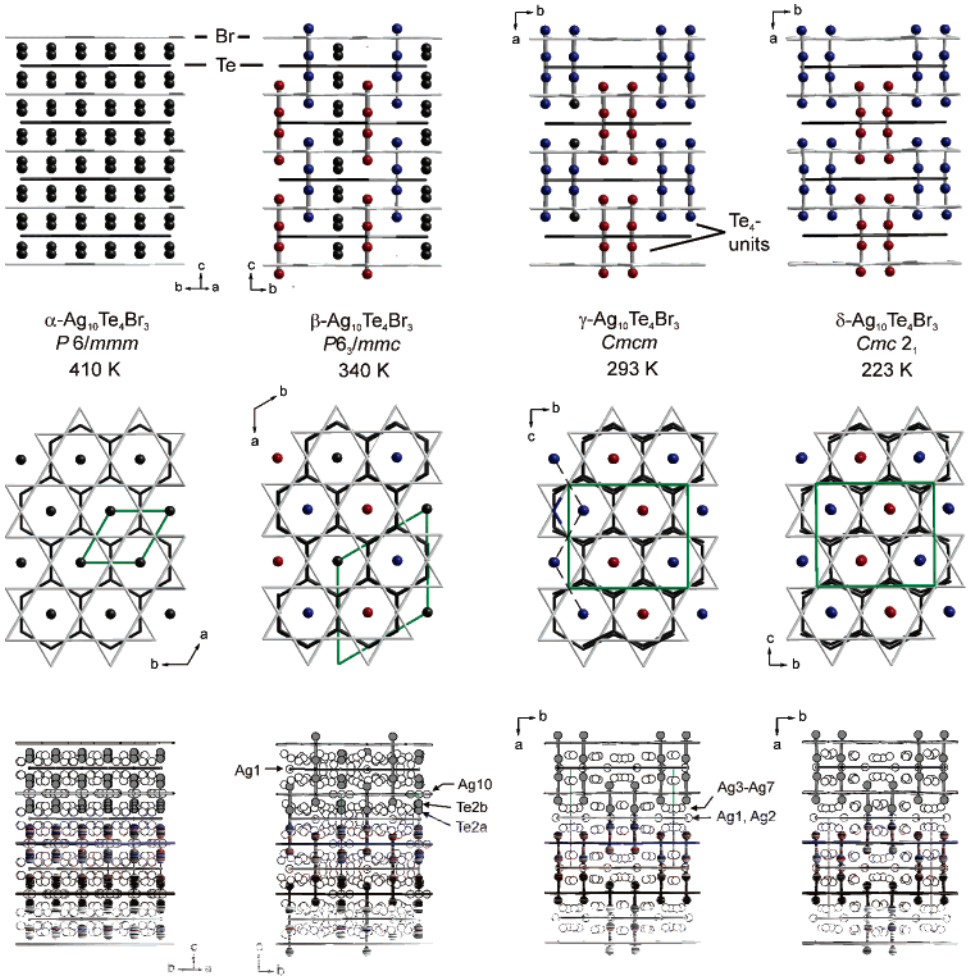

Figure 1. Structure sections of $Ag_{10}Te_4Br_3$. Anion substructure: Te^{2-} (dark gray) and Br^- (light gray) ions are connected by solid lines. 6^3 and 3.6.3.6 nets result from a topological point of view. Areas with predominantly covalently bonded Te_4 units ($[Te_2]^{2-}$ unit + two additional Te^{2-}) are drawn as solid spheres. The translation of the Te_4 units are differentiated by blue and red spheres. At elevated temperature, a structural frustration is generated within the covalently bonded tellurium substructure (gray spheres). The cation substructure is drawn in the bottom section. Unit cells (green solid lines) are drawn for clarity.

compounds[36] and especially for chain structures with super structures, such as Cu_xUTe_3[37] and $RbUSb_{0.33}Te_6$,[38] or square net compounds with modulated structures (RE)$SeTe_2$ (RE = La−Sm)[39] or (RE)Te_3 (RE = Ce−Nd).[40] No hints for twinning or the occurrence of incommensurate modulations could be detected, but diffuse scattering effects were observed for both high-temperature polymorphs. A simple mechanism can be discussed to explain the unusual finding (discussion in the diffuse scattering section).

3.2. Structure Descriptions. The easiest access to the complex crystal structures can be achieved by a separate description of the anion and the cation substructures, also applying a topological description to the anion substructures.

Anion Substructures. Taking distances of *d*(Te−Te) > 4.12 Å and *d*(Br−Br) > 3.7 Å into account, which are equivalent to more than two times the van der Waals radii for each ion according to Pauling,[41] the Br^- ions form Kagomé-like 3.6.3.6 nets and isolated Te^{2-} ions are arranged to form a 6^3 network. Distortions within the nets at low temperatures disappear at higher temperatures to form ideal nets in the high-temperature polymorph. In Figure 1, the two nets are represented by solid lines.

Both nets are stacked alternately along one crystallographic axis in each polymorph. Predominantly covalently bonded tellurium forms a so-called Te_4 unit, represented by a $[Te_2]^{2-}$ dumbbell (*d*(Te−Te) between 2.79 and 2.90 Å) and two additional tellurium atoms at distances well below two times the van der Waals radius of 4.12 Å (*d*(Te−Te) from 3.59 to 3.84 Å, see Table 2). This distance distribution is common for covalent tellurium with dispersive interactions to neighboring atoms and can be found for instance in trigonal tellurium (2.85 and 3.46 Å).[42] Because of significant differences in the chemical bonding of the predominantly covalently bonded Te_4 units compared with the isolated Te^{2-} ions and cooperative structural effects of this tellurium arrangement, the terminus "Te_4 unit" is used from now on

(36) Patschke, R.; Kanatzidis, M. G. *Phys. Chem. Chem. Phys.* **2002**, *4*, 3266.
(37) Patschke, R.; Breshears, J. D.; Brazis, P.; Kannewurf, C. R.; Billinge, S. J. L.; Kanatzidis, M. G. *J. Am. Chem. Soc.* **2001**, *123*, 4755.
(38) Choi, K.-S.; Kanatzidis, M. G. *J. Solid State Chem.* **2001**, *161*, 17.
(39) Tsinde, B. P. F.; Doert, T. *Solid State Sci.* **2005**, *7*, 573.
(40) Malliakas, C.; Billinge, S. J. L.; Kim, H. J.; Kanatzidis, M. G. *J. Am. Chem. Soc.* **2005**, *127*, 6510.
(41) Pauling, L. *The Nature of the Chemical Bond*; Cornell University Press: Ithaca, NY, 1945.
(42) Bradley, A. J. *Philos. Mag.* **1924**, *48*, 477.

Table 2. Distances of the Te_4 Units for α-, *β*-, *γ*- and *δ*-$Ag_{10}Te_4Br_3$

polymorph	*T* (K)	*d*(Te−Te) (Å) $[Te_2]^{2-}$ subunit	*d*(Te−Te) (Å) $[Te_2]^{2-}$ − Te	ordering of Te_4 unit
α-$Ag_{10}Te_4Br_3$	410	2.898(8)	3.809(6)	frustrated
β-$Ag_{10}Te_4Br_3$	340	2.877(9)	3.835(8)	frustrated
		2.793(3)	3.653(3)	ordered
γ-$Ag_{10}Te_4Br_3$	298	2.793(2)	3.604(2)	ordered
δ-$Ag_{10}Te_4Br_3$	223	2.805(1)	3.586(1)	ordered

for ongoing discussions. The Te_4 units form strands interpenetrating the 6^3 telluride and 3.6.3.6 bromide nets parallel to the stacking direction of the networks. In the *δ*- and *γ*-phase, a zigzaglike arrangement of the Te_4 units (see Figure 1, middle section, black fragmented line), shifted relative to each other by a translation vector 1/2 **a**, was observed. In *δ*-$Ag_{10}Te_4Br_3$, a slight bending and reorientation of the Te_4 units relative to the surrounding anion substructure causes a loss of the inversion center and leads to inversion twinning for the low-temperature *δ*-phase. Along the stacking direction of the Te_4 units, silver coordinates the units in an almost linear way to form $[Te_4Ag]_n$ strands (Figure 2).

Going from the *γ*- to the *β*-phase, one-third of the tellurium expected at the Te_4 unit strand position can be described only by half-occupied tellurium positions. The degree of disorder increases to a full disorder for all Te_4 unit strands in the high-temperature α-phase.

A general structure principle of the covalently bonded tellurium substructure has to be developed for $Ag_{10}Te_4Br_3$, valid for all polymorphs. A consistent description must be found that explains the present disorder phenomenon according to this principle. Te_4 units are always located with their covalently bonded $[Te_2]^{2-}$ subunits between two Kagomé Br^- nets, centering the voids of the 6^3 Te^{2-} nets. The end caps of the Te_4 unit interpenetrate the six-membered ring voids of the Kagomé Br nets (see *γ*- and *δ*-$Ag_{10}Te_4Br_3$ in Figure 1). A formation of covalent $[Te_2]^{2-}$ units, centering voids of the Kagomé Br^- nets, is not observed and is not possible because of a resulting low anion−anion distance. According to the translation of the Te_4 units along the stacking direction, two different sets (red and blue spheres in Figure 1) can be defined. A general phase-transition mechanism can be postulated for both the *γ*−*β* and *β*−α phase transitions on the basis of a simple defect-generating mechanism (Figure 3) and structural frustration. The mobility of all silver ions increases with temperature for all polymorphs. In *γ*-$Ag_{10}Te_4Br_3$, on increasing the temperature, the mobility increase led to a depopulation of the strand position (Ag1) between two Te_4 units. Silver is transferred to and delocalized on the silver positions (Ag3−Ag9) located around the 6^3 Te nets. As a consequence, the tellurium has to rearrange, generating a structurally frustrated arrangement of Te_4 units, as illustrated by strands 2 and 2′ in Figure 4. The whole mechanism for the tellurium rearrangement seems to be comparable with a Peierls distortion of a one-dimensional periodic solid, well-known and discussed for many other materials.[43−45]

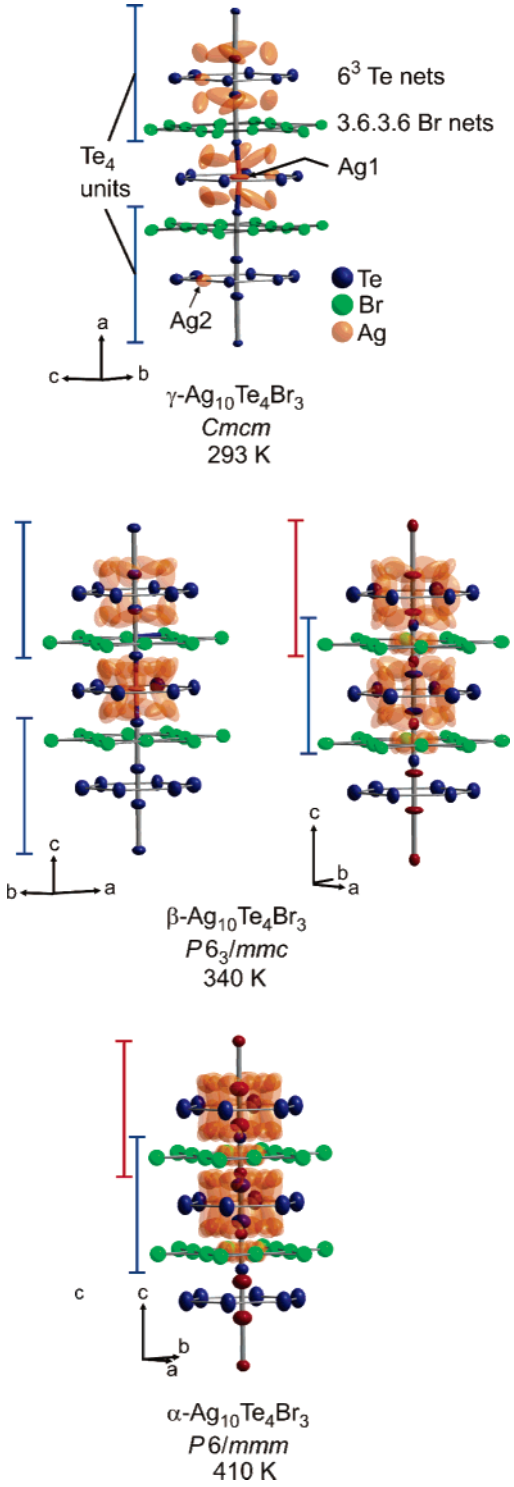

Figure 2. Structure sections featuring the covalently bonded Te_4 units. All $[Te_2]^{2-}$ subunits center voids of the 6^3 tellurium nets with their end caps interpenetrating the 3.6.3.6 bromide nets. An ordered arrangement of Te_4 units, with one silver position (solid orange atom) coordinating two neighbored units in a linear way, is present in *γ*-$Ag_{10}Te_4Br_3$. One-third of the Te_4 units are structurally frustrated in the *β*-phase because of a loss of the linearly coordinating silver (Ag1). A complete frustration was observed for α-$Ag_{10}Te_4Br_3$. Displacement parameters are at 90% probability.

An ongoing depopulation of the silver position generates more structurally frustrated Te_4 unit strands within the tellurium substructure, following the motive of a hexagonal

(43) Decker, A. D.; Landrum, G. A.; Dronskowski, R. Z. *Anorg. Allg. Chem.* **2002**, *628*, 295.
(44) Whangbo, M.-H. In *Crystal Chemistry and Properties of Materials with Quasi-One-Dimensional Structures*; Rouxel, J., Ed.; Reidel: Dordrecht, The Netherlands, 1986.
(45) Whangbo, M.-H.; Hoffmann, R.; Woodward, R. B. *Proc. R. Soc. London, Ser. A* **1979**, *366*, 23.

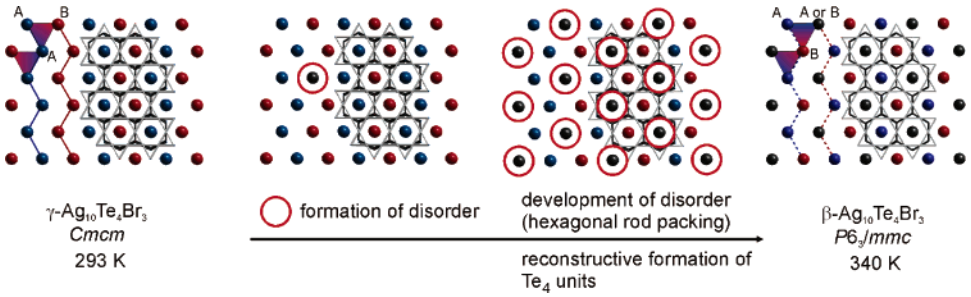

Figure 3. Displacive rearrangement of the Te_4 units observed for the $\gamma-\beta$ phase transition (blue to red).

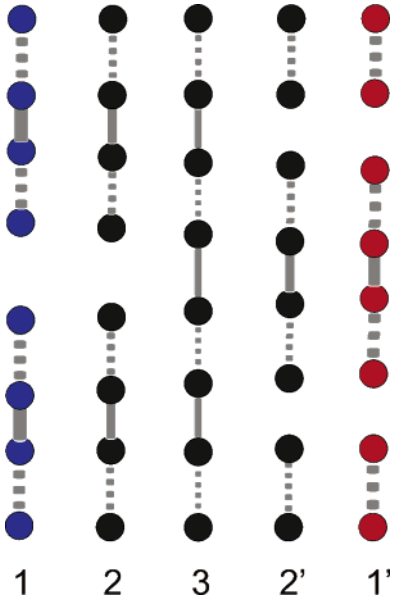

Figure 4. Mechanism of the reconstructive $\gamma-\beta$ phase transition. Structure sections of the predominantly covalently bonded Te_4 units are drawn relative to the 3.6.3.6 bromide (light gray lines) and 6^3 telluride nets. View along the Te_4 rods. Blue and red spheres represent rods of Te_4 units translated relative to each other by half a translation period. Blue and red lines are drawn to clarify the distribution of those rods in the γ-phase. Colored triangles (upper left side in γ-$Ag_{10}Te_4Br_3$) represents the set of AAB arrangements being frustrated in β-$Ag_{10}Te_4Br_3$ (upper left side in β-$Ag_{10}Te_4Br_3$, details see text). Dotted lines represent the former distribution after a reconstructive reorientation of the Te_4 units in the β-phase.

rod packing. Each frustrated strand is neighbored by a nonfrustrated one (Figure 3).

A displacive dislocation of the Te_4 units with breaking covalent tellurium bonds ($[Te_2]^{2-}$ units) and recombination at different positions within the anion substructure is necessary to realize the final arrangement of ordered and structurally frustrated Te_4 units in β-$Ag_{10}Te_4Br_3$. This fact can be derived from the distribution of the crystallographically independent Te_4 units (red and blue in Figure 3) in β-$Ag_{10}Te_4Br_3$ compared with γ-$Ag_{10}Te_4Br_3$. A complete structural frustration of the Te_4 units is realized in the high-temperature α-phase. This general structure principle of hexagonal rod packed Te_4 units is substantiated by the occurrence of diffuse scattering present in the high-temperature forms of $Ag_{10}Te_4Br_3$. A brief discussion is given in the diffuse scattering section.

Cation Substructures. Two general sets of fully occupied silver positions can be identified in the ordered, not frustrated γ-phase, differentiated by the way of coordination to the surrounding anion substructure (Figure 1, bottom section). One set is defined by Ag1 and Ag2, localized within the 6^3 tellurium nets. Ag1 can be found in linear coordination to the Te_4 units (Ag1) centering the hexagonal voids and Ag2 in linear coordination to Te^{2-} positions (Te4) within the 6^3 net. The second set of silver positions (Ag3−Ag7) is arranged between the 6^3 and 3.6.3.6 nets, showing large and anisotropic displacements, defining a 2D area of high mobile silver ions. With increasing silver mobility undergoing the phase transition to the β-phase, the linearly coordinated Ag2 position is completely empty and silver density can be found in direction to the second set of silver positions. The same tendency can be observed for the Ag1 position. Only a certain amount of linearly coordinated Ag1 (occupancy factor 0.74) remains within the Te_4 unit strands, keeping the long-range order intact. An additional silver position (Ag10, occupancy factor 0.21) is realized within the 3.6.3.6 bromide nets of β-$Ag_{10}Te_4Br_3$, increasing the dimensionality of the silver distribution from 2D to 3D.

Ag10 shows a very short and physically meaningless distance of 2.03 Å to the Te1_2b and reasonable distances of 2.80 Å to the Te1_2a and of 2.81 Å to the Br2 position. Bond lengths around 2.80 Å can be found in many other silver telluride materials, e.g., AgTe[46] or $AgAuTe_2$[47] (d(Ag−Te) 2.69 to 2.96 Å), having both covalently bonded and ionic tellurium substructures. The Ag10−Te_2b distance becomes understandable if the structure principle of Te_4 unit rearrangements is applied according to Figure 3. If silver is localized on the Ag10 position, the Te1_2a position cannot be occupied. As a consequence, a population of the Ag10 position can be realized only if two predominantly covalently bonded Te_2 units above and beyond the region of the silver position are present (only Te1_2b position occupied). This situation is equivalent to strand no. 3, middle section of Figure 4, in which the Te_4 unit is rearranged to a strand of slightly elongated Te_2 units. It has to be stated at this point that an equidistant distribution of tellurium along the strand direction, being an logical intermediate step in the postulated structure principle, cannot be realized in any polymorph. Metallic properties, resulting from such an arrangement, could not be detected. The Ag10−Te_2a distance in β-$Ag_{10}Te_4Br_3$ is in very good agreement to the Ag−Te distance of 2.797(1) Å in $(AgI)_2Te_6$, where exclusively covalently bonded Te_6 rings are connected to silver.[48] The interpenetration of silver to the Br-nets also has an effect on the tellurium substructure. For a 3D silver transport, the

(46) Bindi, L.; Spry, P. G.; Cipriani, C. *Am. Mineral.* **2004**, *89*, 1043.
(47) Bindi, L.; Cipriani, C. *Am. Mineral.* **2004**, *89*, 1505.
(48) Deiseroth, H.-J.; Wagener, M.; Neumann, E. *Eur. J. Inorg. Chem.* **2004**, 4755.

rearrangement of the tellurium substructure has to take place contemporaneously to the population of the Ag10 position within the 3.6.3.6 bromide nets. Solid-state NMR spectroscopic measurements are planned to verify this finding. All silver positions in β-$Ag_{10}Te_4Br_3$ are not fully occupied, showing occupancy factors from 0.19 to 0.74.

Going from β-$Ag_{10}Te_4Br_3$ to α-$Ag_{10}Te_4Br_3$, we observe a complete loss of silver density for the linearly coordinating Ag1 position, accompanied by an ongoing tendency of silver to interpenetrate the 3.6.3.6 nets. Nevertheless, a complete isotropic (3D) distribution of silver is not present because the Ag10 position is only slightly occupied (occupancy factor 0.070(2)).

On the opposite side of the temperature spectrum at temperatures below 290 K within the stability region of the δ-phase, the silver mobility is further reduced and silver is distributed over fully occupied positions with splitting of the 16*h* positions in γ-$Ag_{10}Te_4Br_3$ to 8*h* positions in δ-$Ag_{10}Te_4Br_3$.

The structure of $Ag_{10}Te_4Br_3$ is closely related to two other silver polychalcogenides, the mineral stutzite ($Ag_{4.53}Te_3$) and a substitution variant $Ag_{12}Te_6S$.[49,50] In stutzite, an unexpected disorder in parts of the covalently bonded tellurium can be interpreted as being the same type of structural frustration as in the title compound. This structural frustration was eliminated by a partial substitution of tellurium by sulfur in $Ag_{12}Te_6S$.

3.3. Diffuse Scattering and Structural Frustration. Disorder or structural frustration, whether it is static or dynamic in nature, is the origin for diffuse scattering (one randomly selected example is $(Gd,Tb)_{13}Br_{18}B_3$).[51] As a consequence, diffuse scattering has to be observed when the disorder is a real structural property of the material and is not caused by a wrong structure description. Precession plots have been derived from the diffraction data of all polymorphs in order to verify the consequences of the strong frustration phenomena in $Ag_{10}Te_4Br_3$. A projection of two different sets of precession plots (h*x*l and hk*x* with $x = 0$ to 4) is given in Figure 5, with all reciprocal cells drawn with black lines. The pronounced effects of the silver (ion dynamic) and the tellurium (structural frustration) substructures have direct consequences on the diffraction patterns for the α- and β-phase.

Diffuse scattering effects in the form of Kagomé-like nets can be observed, located perpendicular to the c^* direction at *hkl* layers with l = integer $\neq 0$ in β-$Ag_{10}Te_4Br_3$ and at *hk*($l + 0.5$) layers with l = integer > 0 in α-$Ag_{10}Te_4Br_3$. No diffuse scattering effects can be found along the c^* axis for both polymorphs. Red lines in Figure 5 connect the main structure reflections and illustrate the distribution of diffuse scattering intensities for the different polymorphs. The development of the super structure reflections after each phase transition can be estimated from the maxima of diffuse scattering intensities in the previous polymorph.

Exactly the same diffuse scattering phenomena with Kagomé-like scattering effects around the Bragg reflections has been reported for $Na_{22}Ba_{14}CaN_6$ (space group $P6_3/mmc$, $a = 12.666(2)$, $c = 17.554(6)$ Å).[52] Structurally frustrated rods of $Na_6Ba_{14}CaN_6$ clusters along [001], embedded in a honeycomb host structure of sodium atoms, were observed for $Na_{22}Ba_{14}CaN_6$. Steinbrenner and Simon have shown that the disorder in this structure originates from a superimposition of two sets of rods (A and B) at equal weight, located at different heights in *z* within the sodium host. It could be verified that the packing of these rods is not random and follows the motive of a frustrated triangular rod arrangement (ABB or AAB). This situation is well-known for two-dimensional-triangular Ising spin systems when antiferromagnetic interaction leads to spin frustration.[53,54]

The fact that $Ag_{10}Te_4Br_3$ shows exactly the same type of diffuse scattering phenomena leads us to the conclusion that the same statements hold for the explanation of the scattering effects observed here. The high temperature forms of $Ag_{10}Te_4Br_3$ must be regarded as partially and completely frustrated systems of hexagonal rod-packed Te_4 units. Two examples of triangular rod arrangements are given in Figure 4. The phase transitions, driven by the mobility of silver, obviously leaves the Te_4 units intact but creates a partial (β) and complete loss of the long-range order (α) which is defined by the $[Te_4Ag]_n$ rods at lower temperatures. The tellurium distribution along [001] in β- and α-$Ag_{10}Te_4Br_3$, located within the structure areas of the $[Te_4Ag]_n$ rods in γ- and δ-$Ag_{10}Te_4Br_3$, is a superimposition (translation vector 1/2 **c**) of slightly elongated Te_4 units as shown in Figure 4 (dark gray units). Other possibilities like twinning of ordered domains or incommensurate modulations have been excluded (see structure refinement section). Nevertheless, the frustrated Te_4 unit rods must be well-ordered in themselves because of the lack of diffuse scattering effects along the c^* axis in both polymorphs, and only the overall orientation of the Te_4 units relative to the remaining framework is random. Exactly the same behavior was found for $Na_{22}Ba_{14}CaN_6$, in which an illustrative explanation of the theoretical background and a more detailed description of the consequences of frustrated hexagonal rod-packed arrangements are given. A comparable behavior can also be observed in $Ba_{0.6}Sr_{0.4}Al_2O_4$ or $K_2In_{12}Se_{19}$.[55−57]

Consequently, the determination of the averaged structure should be followed by the determination of the real structure by using HRTEM and electron diffraction methods. Unfortunately, the beam instability of those materials refusing such experiments is an intrinsic property of silver-ion-conducting materials.[58] Nevertheless, the "real structure" could be determined by analogy conclusions with other frustrated systems.

3.4. Thermal and Electrical Properties. The thermal behavior of $Ag_{10}Te_4Br_3$ was determined by differential

(49) Peters, J.; Conrad, O.; Bremer, B.; Krebs, B. *Z. Anorg. Allg. Chem.* **1996**, *622*, 1823.
(50) Deiseroth, H.-J.; Mikus, H. *Z. Anorg. Allg. Chem.* **2005**, *631*, *1233.*
(51) Oeckler, O.; Kienle, L.; Mattausch, H. J.; Jarachow, O.; Simon, A. *Z. Kristallogr.* **2003**, *218*, 321.
(52) Steinbrenner, U.; Simon, A. *Z. Kristallogr.* **1997**, *212*, 428.
(53) Ising, E. *Z. Phys.* **1925**, *31*, 253.
(54) Wannier, G. H. *Phys. Rev.* **1950**, *79*, 357.
(55) Fukuda, K.; Iwata, T.; Orito, T. *J. Solid State Chem.* **2005**, *178*, 3662.
(56) Kienle, L.; Simon, A. *J. Solid State Chem.* **2001**, *161*, 385.
(57) Schlosser, M.; Reiner, C.; Deiseroth, H.-J.; Kienle, L. *Eur. J. Inorg. Chem.* **2001**, 2241.
(58) Kienle, L. Personal communication, 2006.

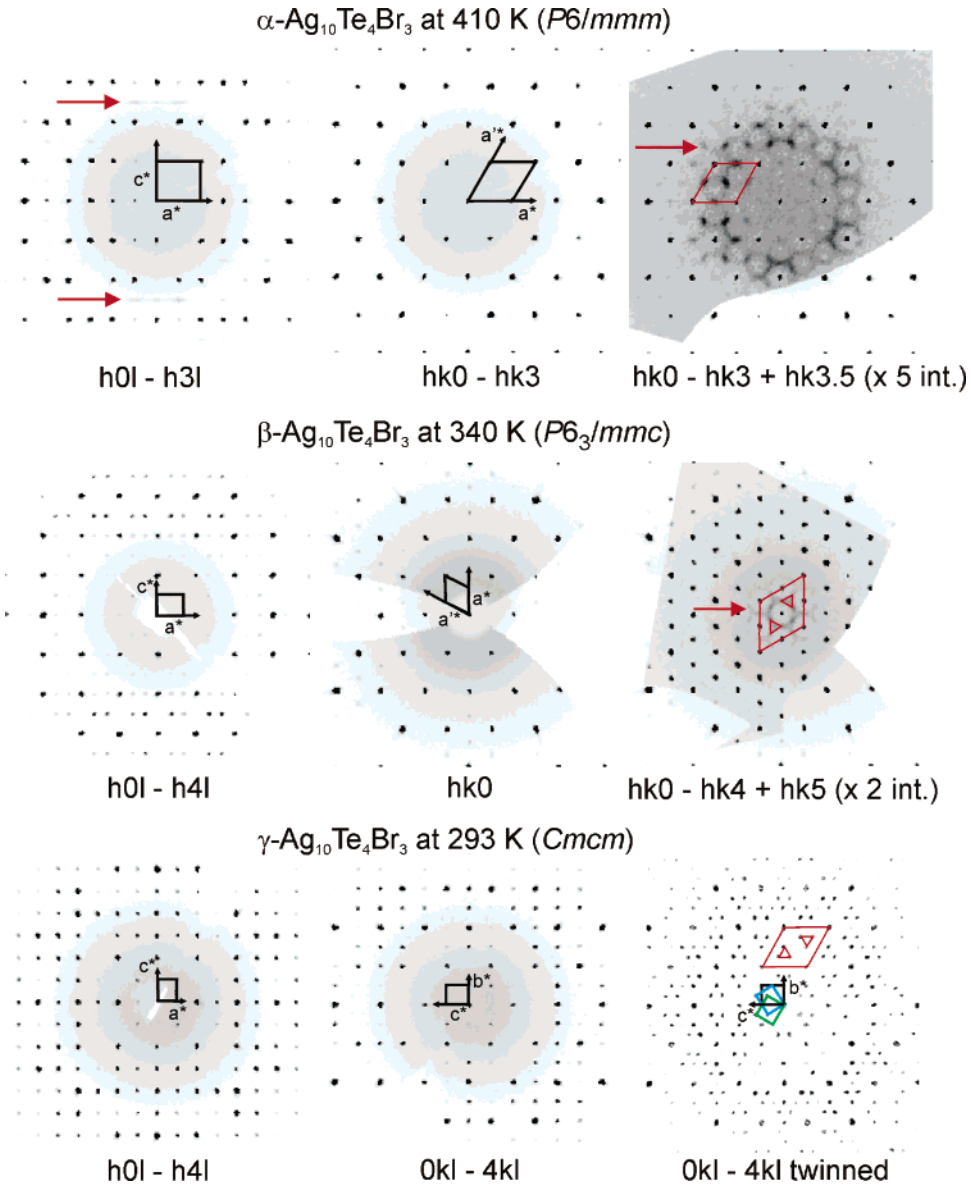

Figure 5. Projections of precession plots for polymorphic $Ag_{10}Te_4Br_3$. Diffuse scattering areas are marked by red arrows in the α- and β-phases. One domain as well as three domain crystals with 1:1:1 twin ratios (right, data from ref 8) can be found for γ-$Ag_{10}Te_4Br_3$. The three reciprocal cells of twinned γ-$Ag_{10}Te_4Br_3$ are drawn in the bottom right section. A close relation between the main Bragg intensities of the α-phase, the combined Bragg and diffuse intensity maxima of the β-phase, and the situation in the γ-phase are illustrated with red lines. Projections of the reciprocal unit-cell dimensions are drawn for each representation. Main structure reflections are emphasized (red lines).

scanning calorimetry (DSC) in the temperature range between 100 and 473 K. Three endothermic effects at 355, 317, and 290 K can be observed that have been assigned to the α−β, β−γ, and γ−δ phase transitions, respectively. Figure 6 and Table 4 give an overview of the effects observed in the temperature range from 173 to 431 K. The three endothermic effects are quite different regarding the shape of the curves and the phase-transition enthalpies. At 290 K, a very small and slightly broadened effect is followed by a sharp and huge effect at 317 K. At 355 K, a broad and textured effect starts that is distributed over a total temperature range of almost 40 K. All effects are reversible according to the temperature values and texture and have been measured from different independently prepared samples in more than two consecutive cycles for each run.

The enthalpy of the first effect is drastically reduced compared with the two following ones, pointing toward a second-order-like phase transition. A first-order-like behavior

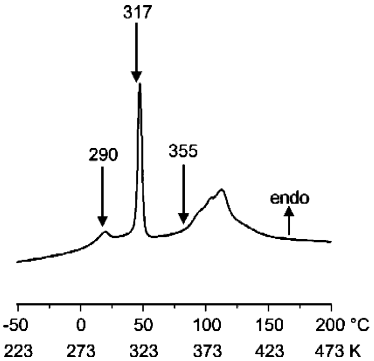

Figure 6. Results from DSC analysis of $Ag_{10}Te_4Br_3$. Section between 223 and 473 K. All thermal effects are reversible in consecutive cycles.

can be postulated for the 317 and 355 K transition. We have assigned the three endothermic thermal effects of $Ag_{10}Te_4Br_3$ to the δ−γ (290 K), γ−β (317 K), and β−α phase transitions. The existence of δ-$Ag_{10}Te_4Br_3$ down to a

Table 3. Results from Thermal Analysis of $Ag_{10}Te_4Br_3$

phase transition	T (onset value) (K)	enthalpy (J g^{-1})
$\alpha-\beta$	355(1)	4.7(1)
$\beta-\gamma$	317(1)	1.9(1)
$\gamma-\delta$	290(1)	0.2(1)

Table 4. Total and Ion Conductivities of Polymorphic $Ag_{10}Te_4Br_3$

phase	T (K)	specific total conductivity (Ω^{-1} cm^{-1})	specific ion conductivity (Ω^{-1} cm^{-1})
α-$Ag_{10}Te_4Br_3$	431		1.1×10^{-1}
	413		9.3×10^{-2}
β-$Ag_{10}Te_4Br_3$	350	1.0×10^{-1}	1.7×10^{-2}
	330	7.0×10^{-2}	8.9×10^{-3}
γ-$Ag_{10}Te_4Br_3$	314	3.1×10^{-2}	1.9×10^{-3}
	301	1.7×10^{-2}	7.5×10^{-4}
δ-$Ag_{10}Te_4Br_3$	223	1.5×10^{-4}	
	173	9.4×10^{-7}	

temperature of 3 K was proven by combined DSC and C_p experiments.

Mixed electronic and ionic conductivity was found for $Ag_{10}Te_4Br_3$. A summary of the total and ionic conductivities for the different polymorphs is given in Table 4. Compared to known silver super ion conductors like AgI, Ag_3SnI_5, Ag_4PbI_6, and Ag_2MI_4 (M = Hg, Cd, Zn),[59] the ionic conductivity of $Ag_{10}Te_4Br_3$ is significantly increased by almost 2 orders of magnitude in the temperature range from 300 to 350 K. Values ranging from approximately 5×10^{-9} (Ag_2ZnI_4) to 5×10^{-5} Ω^{-1} cm^{-1} (AgI) have been reported at 300 K for the above-mentioned series. Even the best ion conductor of this series, Ag_3SnI_5, showing an ionic conductivity of 10^{-4} Ω^{-1} cm^{-1} at 300 K, does not reach the conductivity of $Ag_{10}Te_4Br_3$ (10^{-3} to 10^{-2} Ω^{-1} cm^{-1} at 300 to 350 K). The ionic conductivity of β-$Ag_{10}Te_4Br_3$ is one and a half orders of magnitude lower and that of α-$Ag_{10}Te_4Br_3$ just 1 order of magnitude lower than the ionic conductivity of $RbAg_4I_5$, known to be the best silver super ion conductor at ambient temperatures. Even Ag_3SBr, probably the best candidate for a closely related ion conductor of comparable element composition, has a conductivity that is 1 order of magnitude lower than that in β-$Ag_{10}Te_4Br_3$.[60] Obviously, the introduction of covalent chalcogen substructures drastically optimizes the electrical properties.

Beside the ionic conductivity itself, a halving of the activation energy with temperature can be observed after each phase transition. We have extracted the activation energy from an Arrhenius plot of the ionic conductivities against the reciprocal temperatures as shown in Figure 7. An activation energy of 0.60 eV for γ-$Ag_{10}Te_4Br_3$ is reduced to 0.32 eV for the β-phase and reaches 0.15 eV in α-$Ag_{10}Te_4Br_3$. The latter value is close to the activation energy of 0.08 eV reported for $RbAg_4I_5$,[61] substantiating the huge silver mobility in $Ag_{10}Te_4Br_3$.

Recently, we have shown that the covalently bonded tellurium substructure in γ-$Ag_{10}Te_4Br_3$ is the area of highest ion mobility.[8] The structural frustration of the tellurium

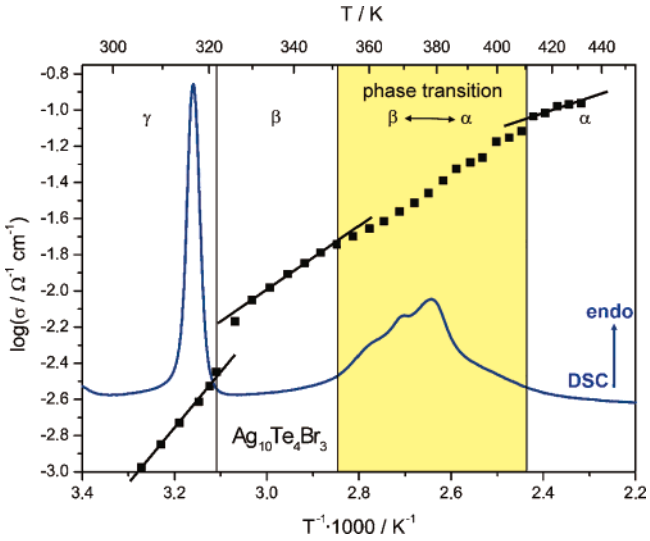

Figure 7. Ionic conductivity in relation to thermal effects for polymorphic $Ag_{10}Te_4Br_3$.

substructure (see structure description) has no drastic influence on the total and partial ion conductivity, as one may see from the development of conductivity while it is undergoing the phase transitions. No drastic effects, such as jumps in the conductivity, were observed during the phase transitions. The continuous change without any steps in the total and ionic conductivity is one of the most promising features of $Ag_{10}Te_4Br_3$. This finding is in contrast to many other silver ion conductors, such as Ag_5Q_2X (Q = Te, Se, S; X = Cl, Br),[34,35] AgI, Ag_3SI,[62] or the above-mentioned AgMI series, where drastic changes in the silver mobility at the order−disorder phase transitions resulted in conductivity jumps of several orders of magnitude.

The total conductivity of $Ag_{10}Te_4Br_3$ exceeds the ionic conductivity by approximately 1 order of magnitude over the whole temperature range (see Table 4). This finding is comparable to $Ag_{4.53}Te_3$, where the same conductivity relation can be found.[63] Because of the high total conductivity and therefore low resistance, high silver ion mobility, and overall stability, $Ag_{10}Te_4Br_3$ seems to be a promising candidate for electrochemical applications.

5. Conclusion and Outlook

$Ag_{10}Te_4Br_3$ represents the first fully characterized coinage metal (poly)chalcogenide halide with four polymorphs in the temperature range of 3−410 K. A combination of temperature-dependent X-ray and thermal analysis led to a complete overview of the structural features and the complex silver dynamic in this new material. A pronounced silver dynamic is the origin of complex disorder phenomena, causing diffuse scattering in the high-temperature α- and β-phases. The diffuse scattering could be addressed by the occurrence of structural frustration comparable with a Peierls-type distortion within the predominantly covalent tellurium substructure. A simple and illustrative structure principle was derived from the $Ag_{10}Te_4Br_3$ structures, mainly on the basis of a topologic description of the rigid ionic chalcogen and halogen sub-

(59) Hull, S.; Keen, D. A.; Berastegui, P. *J. Phys. Condens. Matter* **2002**, *14*, 13579−13596.
(60) Kawamura, J.; Shimoji, M.; Hishino, H. *J. Phys. Soc. Jpn.* **1981**, *50*, 194.
(61) Hull, S.; Keen, D. A.; Sivia, D. S.; Berastegui, P. *J. Solid State Chem.* **2002**, *165*, 363−371.
(62) Agrawal, R. C.; Gupta, R. K. *J. Mater. Sci.* **1999**, *34*, 1131.
(63) Gobec, M.; Sitte, W. *J. Alloys Compd.* **1995**, *220*, 152−156.

structure interpenetrated by predominantly covalent substructure units. Unusual disorder phenomena, like that in the mineral stutzite, can be understood by this structure principle.

Temperature-dependent impedance experiments and solid-state NMR spectroscopy are currently underway to examine the dynamic properties in more detail. In particular, ^{109}Ag− and ^{125}Te−NMR spectroscopic experiments around the $\alpha-\beta$ phase transition of $Ag_{10}Te_4Br_3$ are promising interesting results due to the drastic changes in the silver and tellurium substructures over a wide temperature range. Particularly, the answer to the question whether the rearrangement in the tellurium substructure is dynamic or static in nature will be addressed soon.

Acknowledgment. This work was financed by the DFG in the SFB 458 'Ionic motion in materials with Disordered Structures'. Use of the DSC equipment of Prof. H. Eckert, University of Münster, and preparation of DSC measurements by W. Pröbsting are gratefully acknowledged. We thank Dr. S. Rayaprol for performing the C_p measurements and J. M. Deckwart for technical support concerning the electrochemical measurements.

Supporting Information Available: The Supporting Information has been sent to the Fachinformationzentrum Karlsruhe, Abt. PROKA, 76344 Eggenstein-Leopoldshafen, Germany, as CSD 417272 (α-$Ag_{10}Te_4Br_3$), 417271 (β-$Ag_{10}Te_4Br_3$), 417273 (γ-$Ag_{10}Te_4Br_3$), and 417274 (δ-$Ag_{10}Te_4Br_3$), and can be obtained by contacting the FIZ (quoting the article details and the corresponding CSD number). An overview of the refinement strategies, further crystallographic data of $Ag_{10}Te_4Br_3$, CIF files, and C_p data. This material is available free of charge via the Internet at http://pubs.acs.org.

CM062731P